This is a preprint, the final version is subject to change, of the American Mineralogist (MSA)
Cite as Authors (Year) Title. American Mineralogist, in press.
DOI: https://doi.org/10.2138/am-2020-7349
Revision 2 of manuscript (#7349) submitted to *American Mineralogist*

Density and sound velocity of liquid Fe–S alloys at Earth's outer core conditions

Jie Fu[1*], Lingzhi Cao[1], Xiangmei Duan[1*], and Anatoly B. Belonoshko[2]

[1] Department of Physics, School of Physical Science and Technology, Ningbo University, 315211 Ningbo, China.

[2] Department of Physics, AlbaNova University Center, Royal Institute of Technology (KTH), 106 91 Stockholm, Sweden.

Corresponding authors: Jie Fu (fujie@nbu.edu.cn), Xiangmei Duan (duanxiangmei@nbu.edu.cn)

Key Points:

- First-principles molecular dynamics simulations of liquid Fe–S alloys are performed at the Earth's outer core conditions.
- *P–T–V* equations of state for liquid Fe–S alloys are established.
- Density and sound velocity of liquid Fe–S alloys along the geotherm are estimated.
- S concentration in the outer core is constrained.

Abstract

Pressure–temperature–volume (P–T–V) data on liquid iron–sulfur (Fe–S) alloys at the Earth's outer core conditions (~ 136 to 330 GPa, ~ 4000 to 7000 K) has been obtained by first-principles molecular dynamics simulations. We developed thermal equation of state (EOS) composed of Murnaghan and Mie-Grüneisen-Debye expressions for liquid Fe–S alloys. The density and sound velocity are calculated and compared with Preliminary Reference Earth Model (PREM) to constrain the S concentration in the outer core. Due to the temperature at the inner core boundary (T_{ICB}) has not been measured precisely (4850 ~ 7100 K), we clarify that the S concentration range is from 10 ~ 14 wt.% assuming S is the only light element. Our results also show that Fe–S alloy couldn't satisfy the seismological density and sound velocity simultaneously. S element couldn't be the only light element. Considering the geophysical and geochemical constrains, we propose the outer core contains no more than 3.5 wt.% S, 2.5 wt.% O, or 3.8 wt.% Si. In addition, the developed thermal EOS can be utilized to calculate plenty of thermal properties of liquid Fe–S alloys serving as fundamental data to model the Earth's outer core.

1 Introduction

The composition of the Earth's outer core with pressure from 136 to 330 GPa and temperature from 4000 to 7000 K (Dziewonski and Anderson 1981; Koči et al. 2007; Alfè 2009) remains controversial. The direct geophysical data is from measuring the speed of seismic wave propagation. Understanding the geodynamics in the outer core highly requires the thermal properties of its composition. According to Birch's reports (Birch 1952), the outer core is mainly composed of iron (Fe). While Preliminary Reference Earth Model (PREM) (Dziewonski and Anderson 1981) raises that pure Fe is much denser than the substance in outer core, and has a lower sound velocity. It's argued that there must exist some light elements (e.g. sulfur, silicon, oxygen, carbon, and hydrogen) to decrease the density and increase sound velocity (Poirier 1994; Hirose et al. 2013; Badro et al. 2015; Litasov and Shatskiy 2016; Umemoto and Hirose 2020). The presence of light elements dose reduce the density of ferroalloy, but not the sound velocity of each component matches the PREM data. The type of light elements is still pending.

Owing to its siderophile nature, sulfur (S) is considered as a major light element in the Earth's outer core (Huang et al. 2011; Kawaguchi et al. 2017). The concentration of S is typically predicted by comparing the density and sound velocity of liquid Fe–S alloy with PREM data. So far, many efforts have been done in experiment. Huang and co-authors (Huang et al. 2011, 2018) measured the density and sound velocity of liquid $Fe_{92.5}O_{2.2}S_{5.3}$ and $Fe_{90}O_8S_2$ up to 208 GPa and Fe–11.8 wt.% S up to 211.4 GPa through the shock-wave experiment and predicted the maximum S content was around 10 wt.%. A similar experiment estimated the S concentration of 2 wt.% (Zhang et al. 2016). Using laser heated diamond-anvil cells device, Kawaguchi et al. measured the sound velocity of $Fe_{47}Ni_{28}S_{25}$ and $Fe_{63}Ni_{12}S_{25}$ up to 58 GPa and 2480 K, and proposed the amount of S was 5.8 ~ 7.5 wt.% (Kawaguchi et al. 2017). Since most experimental *P–T–V* data (Sanloup et al. 2002; Badro et

al. 2007; Jing et al. 2014; Kuskov and Belashchenko 2016) is measured at pressure and/or temperature below the outer core conditions, the values at high $P–T$ are usually extrapolated from Birch's law (Badro et al., 2007). The validity of birch's law at extremely high temperatures is questionable (Lin et al. 2005). In brief, due to technical challenges in dynamic and static high-pressure measurement, the exact S concentration in the Earth's outer core is far from reaching a consensus.

As a remedy, theoretical calculations has been utilized to identify the S concentration (Alfè and Gillan 1998; Alfè et al. 2002a; Badro et al. 2014; Umemoto et al. 2014; Bazhanova et al. 2017). Since some theoretical calculations are performed at zero K, temperature effects on thermal pressure are often neglected or approximated (Bazhanova et al. 2017). Ignoring the temperature impact at extreme conditions leads to erroneous pressure-volume ($P–V$) relationship. Therefore, first-principles molecular dynamics (FP-MD) simulations are suitable to study the $P–T–V$ relations, namely, equation of state (EOS). Applied with the EOS, density and sound velocity can be obtained. Actually, the thermal EOS for liquid Fe has been reported (Vočadlo et al. 2003; Bouchet et al. 2013; Ichikawa et al. 2014; Wagle and Steinle-Neumann 2019), whereas it is rare for liquid Fe–S alloys. The latter plays a central role on predicting the S concentration in the outer core.

In this work, the $P–T–V$ data of liquid Fe–S alloys with different S concentrations (0, 5.5, 11.5, and 18.1 wt.%) are obtained by FP-MD simulations with pressure and temperature up to 330 GPa and 7000 K. We establish thermal EOS for liquid Fe–S alloys, and then calculate the density and sound velocity along the geotherm of the outer core. In order to constrain S content, the current data is compared to PREM data. Besides, the density and sound velocity of liquid Fe–S alloys provided by FP-MD calculations are fundamental to build geophysical and geochemical model of the Earth's outer core.

2 Computational Methods

FP-MD are based on the density functional theory (DFT) as implemented in the Vienna Ab initio Simulation Package (VASP) (Kresse and Hafner 1993; Kresse and Furthmüller 1996). The exchange-correlation functional is the Perdew-Burke-Ernzerhof (PBE) (Perdew et al. 1996) variant of the generalized gradient approximation (GGA). Projector augmented wave (PAW) pseudopotentials (Blöchl 1994) use fourteen valence electrons ($3p^6 3d^7 4s^1$) with the outmost cutoff radius (r_c) 2.2 a.u. for iron, and six valence electrons ($3s^2 3p^4$) with r_c = 1.5 a.u. for sulfur to avoid state overlapping under high temperature and pressure conditions. Valence electrons states are expanded into plane waves with a cutoff energy of 500 eV. The finite temperatures for electronical structure and force calculations are implemented within the Fermi-Dirac smearing (Mermin 1965). The reciprocal Brillouin zone is sampled by gamma point. These setting values are sufficient to produce converging results. Molecular dynamics runs have been performed in the canonical ensemble (NVT) using Nosè-Hoover thermostat (Nosé 1984; Hoover 1985) to control the temperature. Every simulation runs for 7 ps with timestep 1.0 fs. The first 2 ps are to reach the equilibrium. *P* and *T* values are averaged statistically from the last 5 ps. By the block method (see the supplementary material part), the estimated statistic errors of pressure are within 0.35 GPa. The running steps are long enough to collect accurate averages.

The initial configuration of liquid Fe including 108 atoms is built by melting the perfect face-centered cubic (fcc) phase Fe with density of 11.893 g/cm^3 at 10000 K for 10 ps. The liquid state is confirmed by the Fe–Fe radial distributional function (RDF) and mean square displacement (MSD) of Fe atoms, which increases with time in liquid and is a constant in solid fcc Fe (see Fig. S3). The initial configurations of liquid Fe–S alloys are obtained via randomly replacing Fe atoms by S to reach the target S concentration, melted at 10000 K for

10 ps, and then quenched to target temperature. Different pressures are obtained by varying the box size.

3 Results and discussions

In this work, we study four concentrations of S (0, 5.5, 11.5, and 18.1 wt.%) of liquid Fe–S alloys at pressure ranges from 136 to 330 GPa and temperature from 4000 to 7000 K. Figure 1 shows the comparison of isothermal density of liquid Fe at 6000 K with previous available data (Brown and McQueen 1986; Anderson and Ahrens 1994; Dewaele et al. 2006; Umemoto et al. 2014). It is clearly seen that the density of liquid Fe is slightly higher than values by EOS fitted to experimental thermal expansion, enthalpy, and sound velocity etc. (Anderson and Ahrens 1994), and lower than DFT values (Umemoto et al. 2014). The derivations are within 1.2% and 1.4%, respectively. We state that the difference with previous DFT calculation is possibly caused by technical details (e.g. cell size, exchange-correlation functional, pseupotential parameters, and so on). Compared with shock-wave compression density 12.44 g/cm^3 at 260 GPa and 6069 K (Brown and McQueen 1986), the calculated value is 12.30 g/cm^3 with derivation around 1.13 %. It's comparable to the experimental uncertainty. The agreement confirms the FP-MD data is reliable.

To calculate thermal properties at given P and T, the EOS of liquid Fe–S alloys are indispensable. Here, the P–T–V relations are analyzed combining Murnaghan (Murnaghan 1944) and Mie-Grüneisen-Debye (MGD) EOS (Ichikawa et al. 2014)

$$P(V,T) = P_{T_0}(V) + \Delta P_{th}(V,T), \quad (1)$$

$P(V,T)$ is the total pressure, P_{T_0} is the pressure at a reference temperature T_0. P_{T_0} is expressed as Murnaghan EOS (Murnaghan 1944)

$$P_{T_0} = \frac{K_{T_0}}{K'_{T_0}}\left[\left(\frac{V_0}{V}\right)^{K'_{T_0}} - 1\right], \quad (2)$$

K_{T_0} is thermal bulk modulus at zero pressure and K'_{T_0} is the derivative of K_{T_0} over pressure at T_0. V_0 is the volume at zero pressure. The thermal pressure ΔP_{th} is expressed as

$$\Delta P_{th}(V,T) = \frac{\gamma(V)}{V}\left(E(V,T) - E(V,T_0)\right), \quad (3)$$

$\gamma(V)$ is Grüneisen parameter. Here we assume $\gamma(V) = \gamma_0$ that is independent with pressure and temperature in the target P–T range. The internal thermal energy $E(V,T)$ is represented by a second-order polynomial of temperature with a volume dependent second-order coefficient as

$$E = 3nR\left[T + e_0\left(\frac{V}{V_0}\right)^g T^2\right], \quad (4)$$

where R is the gas constant (R = 8.314 J·mol^{-1}·K^{-1}) and n is the number of atoms in the formula unit (Fe: n = 1; Fe–S: n = 2). The first term corresponds to atomic contribution, while the second term represents the electronic contribution.

The present EOS is comprised of four equations, which requires six parameters (V_0, K_{T_0}, K'_{T_0}, γ_0, e_0, and g) to calculate the pressure. These parameters are fitted to the FP-MD P–T–V data by least squares algorithm (see Table 1.). We set the temperature 6000 K as the reference temperature T_0 in order to constrain the reference isotherm as tightly as possible in the broad P–T range. We discuss the accuracy of Murnaghan EOS to describe the isothermal pressure in the supplementary material part.

How does the introduction of S change the thermal properties of liquid Fe alloy? The isothermal density of liquid Fe–S alloys is presented in Figure 2. The general trend is the density decreases with temperature and S concentration. It is consistent with the conclusions about liquid Fe–S and Fe–H alloys (Umemoto et al. 2014; Umemoto and Hirose 2015). The results indicate the density of Fe–11.5 wt.% S composition is close to the PREM data.

Based on the EOS, we calculate thermal properties including isothermal bulk modulus (K_T), adiabatic bulk modulus (K_S), and sound velocities (V_P) of liquid Fe–S alloys. The isothermal bulk modulus (K_T) is defined by $K_T = -V\left(\frac{\partial P}{\partial V}\right)_T$. The adiabatic bulk modulus (K_S) is determined by $K_S = (1+\alpha\gamma T)K_T$, where α is volumetric thermal expansion coefficient. αK_T is both temperature and volume dependent and can be calculated by $\alpha K_T = (\frac{\partial P}{\partial T})_V$. The calculated αK_T values of Fe–S alloys at different P and T are listed in Table S1. For liquid Fe, αK_T = 0.011 GPa K^{-1} at 80 GPa, 2500 K (Seagle et al. 2006), and $\alpha K_T = 0.95\times10^{-2}$ at 150 GPa and 4000 K (Ichikawa et al. 2014). Here we get αK_T = 0.01162 GPa K^{-1} for Fe at 4000 K that is in good agreement with previous reports. We assume Grüneisen parameter γ_0 = 1.5 based on previous first-principles calculations and experimental measurements (Brown and McQueen 1986; Anderson and Ahrens 1994; Wasserman et al. 1996; Alfè et al. 2002b; Belonoshko 2010). The value is widely used in reported experimental or theoretical analysis on the similar issue (Huang et al. 2011; Umemoto et al. 2014). The sound velocity V_P of liquid Fe–S alloys is calculated by $V_P = \sqrt{\frac{K_S}{\rho}}$, where ρ is the density of the substance. The uncertainty of sound velocity mainly caused by Grüneisen parameter is within 1.79 %.

In the following, we compare the isothermal sound velocity of liquid Fe–S alloys with PREM (see Figure 3). Obviously, it increases with pressure. Introducing S atoms into liquid Fe alloy does increase the sound velocity. The curves of Fe–5.5 wt.% S are close to the PREM data. Combined to the density- and sound velocity-pressure relations, the likely S concentration should be between 5.5 and 11.5 wt.%. In addition, the results (see solid lines) also indicate that sound velocity is insensitive to temperature. The same conclusion was

reported in the study of liquid Fe–S and Fe–H alloy (Umemoto et al. 2014; Umemoto and Hirose 2015).

4 Geophysical implications

Based on the Murnaghan-MGD EOS, we estimate the S concentration in the outer core. The adiabatic temperature profile along the geotherm is given by

$$T = T_{ICB}\left(\frac{\rho}{\rho_{ICB}}\right)^{\gamma}, \quad (5)$$

where T_{ICB} and ρ_{ICB} are temperature and density at the inner core boundary (ICB), ρ is the density. γ is Grüneisen parameter.

It is known that T_{ICB} relies closely on melting temperature (T_{m}) of Fe at ICB pressure. According to different approaches, T_{m} varies from 4850 K by extrapolation of static compression measurement (Boehler 1993), 6230±500 K by fast x-ray diffraction (Anzellini et al. 2013) to 5400 ~ 7100 K via first-principles or semi-classical calculations (Wasserman et al. 1996; Stixrude et al. 1997; Belonoshko et al. 2000; Laio et al. 2000; Alfè 2009; Belonoshko et al. 2017, 2019). Since T_{m} at ICB pressure has not been measured precisely, four anchoring temperatures of 4850 K (Boehler 1993), 5400 (Laio et al. 2000), 6350 (Alfè 2009; Anzellini et al. 2013), and T_{ICB} 7100 (Belonoshko et al. 2000) are tested to estimate the temperature at the core mantle boundary (CMB). The adiabatic temperature profiles are presented in Figure 4, and the corresponding T_{CMB} are 3562, 3966, 4664, and 5214 K, respectively.

We elaborate on the density and sound velocity profiles for S concentration 5.5 ~ 11.5 wt.% ferroalloy along the geotherm with T_{ICB} = 4850, 5400, 6350, and 7100 K, as displayed in Figure 5., The most possible Fe–S alloy composition in the outer core is then predicted. If T_{ICB} is around 4850 K (Boehler 1993), we predict Fe–14.0 wt.% S reproduce the density of

192 PREM data by interpolation. With T_{ICB} around 5400 K (Laio et al. 2000), it is Fe–13.0 wt.%
193 S that reproduce the PREM density profile. Applied with the same T_{ICB}, previous first-
194 principles approach estimated the maximum S concentration was 14 wt.% (Umemoto et al.
195 2014) while shock-wave compression experiment (Huang et al. 2013, 2018) gave out 10.0
196 wt.%. Our result is comparable with previous first-principles one within the calculation
197 deviation. Another well agreed T_{ICB} by both theory (Alfè 2009) and experiment is around
198 6350 K (Anzellini et al. 2013). Estimated with this value, it is Fe–11.5 wt.% S that could
199 reproduce the PREM density profile. Since recent first-principles calculations argued a
200 "high" T_m (~ 7100 K) of Fe (Belonoshko et al. 2000, 2017, 2019), we apply T_{ICB} = 7100 K to
201 estimate the S concentration in the outer core and find that Fe–10 wt.% S could explain the
202 PREM density quite well.

203 As the Figure 5 shown, the sound velocity along the geotherm increases with the
204 sulfur concentration and is insensitive with the T_{ICB} temperature. Our predicted slopes of
205 sound velocity versus pressures are in good agreement with the PREM one and better than
206 the ones from previous first-principles approach (Umemoto et al. 2014) and shock-wave
207 compression experiment (Huang et al. 2013, 2018). It should be noted that the predicted
208 sound velocity of liquid Fe–S alloys in this work is still higher than PREM data by about
209 1.74 % at the bottom and 3.04% at the top of the outer core.

210 Since Fe–S alloy can't match the deficits in density and sound velocity
211 simultaneously, there must be other light elements in the outer core, for example, oxygen or
212 silicon. Earlier first-principles calculation (Badro et al. 2014) showed that the outer core must
213 contain oxygen to synchronously satisfy the seismological density and sound velocity.
214 However, the shock-wave compression experiment (Huang et al. 2011) ruled out oxygen as a
215 major light element and stated oxygen concentration should be less than 2.5 wt.%. Recent
216 experiment with the same method reported that 9.0 wt.% Si in the outer core and 3.8 wt.% Si

in the inner core could match the PREM data (Huang et al. 2019). Besides, melting experiment demonstrated eutectic liquid in Fe–Fe_3S binary system contains less than 15 wt.% S at 15 GPa (Fei et al. 2000), 9.5 wt.% S at 136 GPa (CMB pressure), or 6.0 wt.% S at 254 GPa (Mori et al. 2017). One pace further, we deduce the S partition at 330 GPa (ICB pressure) is approximately 3.5 wt.%. Combination of the geophysical and geochemical constrains, we propose the outer includes no more than 3.5 wt.% S, 2.5 wt.% O, or 3.8 wt.% Si. Detailed calculations about the density and sound velocity of Fe–S–O–Si alloys should be performed in future work.

Acknowledgments

The authors acknowledge support from the National Natural Science Foundation of China (NSFC) (Grant No: 11804175 and No. 11874033), the K.C. Wong Magna Foundation in Ningbo University. A. B. is thankful to the Swedish Research Council (VR) for financial support (grant 2017-03744). J. F. thanks Yunguo Li from University College of London for discussions. Computations were performed using the facilities at the Swedish National Infrastructure for Computing (SNIC) located at NSC in Linköping. The data can be achieved from mendeley data repository (https://data.mendeley.com/datasets/b8t6j2yd3k/1).

References

Alfè, D. (2009) Temperature of the inner-core boundary of the Earth: Melting of iron at high pressure from first-principles coexistence simulations. Physical Review B, 79, 1–4.

Alfè, D., and Gillan, M.J. (1998) First-principles simulations of liquid Fe-S under Earth's core conditions. Physical Review B, 58, 8248–8256.

Alfè, D., Gillan, M.J., and Price, G.D. (2002a) Composition and temperature of the earth's core constrained by combining ab initio calculations and seismic data. Earth and Planetary Science Letters, 195, 91–98.

Alfè, D., Price, G., and Gillan, M. (2002b) Iron under Earth's core conditions: Liquid-state thermodynamics and high-pressure melting curve from ab initio calculations. Physical Review B, 65, 165118.

Anderson, W.W., and Ahrens, T.J. (1994) An equation of state for liquid iron and implications for the Earth's core. Journal of Geophysical Research, 99, 4273–4284.

Anzellini, S., Dewaele, A., Mezouar, M., Loubeyre, P., and Morard, G. (2013) Melting of iron at Earth's inner core boundary based on fast X-ray diffraction. Science, 340, 464–466.

Badro, J., Fiquet, G., Guyot, F., Gregoryanz, E., Occelli, F., Antonangeli, D., and d'Astuto, M. (2007) Effect of light elements on the sound velocities in solid iron: Implications for the composition of Earth's core. Earth and Planetary Science Letters, 254, 233–238.

Badro, J., Cote, A.S., and Brodholt, J.P. (2014) A seismologically consistent compositional model of Earth's core. Proceedings of the National Academy of Sciences, 111, 7542–7545.

Badro, J., Brodholt, J.P., Piet, H., Siebert, J., and Ryerson, F.J. (2015) Core formation and core composition from coupled geochemical and geophysical constraints. Proceedings of the National Academy of Sciences of the United States of America, 112, 12310–12314.

Bazhanova, Z.G., Roizen, V. V., and Oganov, A.R. (2017) High-pressure behavior of the Fe-S system and composition of the Earth's inner core. Uspekhi Fizicheskih Nauk, 187, 1105–1113.

Belonoshko, A.B. (2010) Equation of state for ∈-iron at high pressures and temperatures. Condensed Matter Physics, 13, 23605–23615.

Belonoshko, A.B., Ahuja, R., and Johansson, B. (2000) Quasi–Ab Initio Molecular Dynamic Study of Fe Melting. Physical Review Letters, 84, 3638–3641.

Belonoshko, A.B., Lukinov, T., Fu, J., Zhao, J., Davis, S., and Simak, S.I. (2017) Stabilization of body-centred cubic iron under inner-core conditions. Nature Geoscience, 10, 312.

Belonoshko, A.B., Fu, J., Bryk, T., Simak, S.I., and Mattesini, M. (2019) Low viscosity of the Earth's inner core. Nature Communications, 10, 2483.

Birch, F. (1952) Elasticity and constitution of the Earth's interior. Journal of Geophysical Research, 57, 227–286.

Blöchl, P.E. (1994) Projector augmented-wave method. Physical Review B, 50, 17953–17979.

Boehler, R. (1993) Temperatures in the Earth's core from melting-point measurements of iron at high-static pressures. Nature, 363, 534–536.

Bouchet, J., Mazevet, S., Morard, G., Guyot, F., and Musella, R. (2013) Ab initio equation of state of iron up to 1500 GPa. Physical Review B, 87, 1–8.

Brown, J.M., and McQueen, R.G. (1986) Phase transitions, Gruneisen parameter, and elasticity for shocked iron between 77 GPa and 400 GPa. Journal of Geophysical Research, 91, 7480–7494.

283 Dewaele, A., Loubeyre, P., Occelli, F., Mezouar, M., Dorogokupets, P.I., and Torrent, M.
284 (2006) Quasihydrostatic Equation of State of Iron above 2 Mbar. Physical Review
285 Letters, 97, 215504.
286 Dziewonski, A.M., and Anderson, D.L. (1981) Preliminary reference Earth model. Physics of
287 the Earth and Planetary Interiors, 25, 297–356.
288 Fei, Y., Li, J., Bertka, C.M., and Prewitt, C.T. (2000) Structure type and bulk modulus of
289 Fe3S, a new iron-sulfur compound. American Mineralogist, 85, 1830–1833.
290 Hirose, K., Labrosse, S., and Hernlund, J. (2013) Composition and State of the Core. Annual
291 Review of Earth and Planetary Sciences, 41, 657–691.
292 Hoover, W.G. (1985) Canonical dynamics: Equilibrium phase-space distributions. Physical
293 Review A, 31, 1695–1697.
294 Huang, H., Fei, Y., Cai, L., Jing, F., Hu, X., Xie, H., Zhang, L., and Gong, Z. (2011)
295 Evidence for an oxygen-depleted liquid outer core of the Earth. Nature, 479, 513–516.
296 Huang, H., Wu, S., Hu, X., Wang, Q., Wang, X., and Fei, Y. (2013) Shock compression of
297 Fe-FeS mixture up to 204 GPa. Geophysical Research Letters, 40, 687–691.
298 Huang, H., Leng, C., Wang, Q., Yang, G., Hu, X., Wu, Y., Liu, X., and Fei, Y. (2018)
299 Measurements of Sound Velocity of Liquid Fe-11.8 wt % S up to 211.4 GPa and
300 6,150 K. Journal of Geophysical Research: Solid Earth, 123, 4730–4739.
301 Huang, H., Leng, C., Wang, Q., Young, G., Liu, X., Wu, Y., Xu, F., and Fei, Y. (2019)
302 Equation of State for Shocked Fe-8.6 wt % Si up to 240 GPa and 4670 K. Journal of
303 Geophysical Research: Solid Earth, 124, 8300–8312.
304 Ichikawa, H., Tschuchiya, T., and Tange, Y. (2014) The P-V-T equation of state and
305 thermodynamic properties of liquid iron. Journal of Geophysical Research: Solid Earth,
306 119, 240–252.

Jing, Z., Wang, Y., Kono, Y., Yu, T., Sakamaki, T., Park, C., Rivers, M.L., Sutton, S.R., and Shen, G. (2014) Sound velocity of Fe-S liquids at high pressure: Implications for the Moon's molten outer core. Earth and Planetary Science Letters, 396, 78–87.

Kawaguchi, S.I., Nakajima, Y., Hirose, K., Komabayashi, T., Ozawa, H., Tateno, S., Kuwayama, Y., Tsutsui, S., and Baron, A.Q.R. (2017) Sound velocity of liquid Fe-Ni-S at high pressure. Journal of Geophysical Research: Solid Earth, 122, 3624–3634.

Koči, L., Belonoshko, A.B., and Ahuja, R. (2007) Molecular dynamics calculation of liquid iron properties and adiabatic temperature gradient in the Earth's outer core. Geophysical Journal International, 168, 890–894.

Kresse, G., and Furthmüller, J. (1996) Efficient iterative schemes for ab initio total-energy calculations using a plane-wave basis set. Physical Review B, 54, 11169–11186.

Kresse, G., and Hafner, J. (1993) Ab initio molecular dynamics for liquid metals. Physical Review B, 47, 558–561.

Kuskov, O.L., and Belashchenko, D.K. (2016) Thermodynamic properties of Fe-S alloys from molecular dynamics modeling: Implications for the lunar fluid core. Physics of the Earth and Planetary Interiors, 258, 43–50.

Laio, A., Bernard, S., Chiarotti, G.L., Scandolo, S., and Tosatti, E. (2000) Physics of Iron at Earth's Core Conditions. Science, 287, 1027–1030.

Lin, J.F., Sturhahn, W., Zhao, J., Shen, G., Mao, H.K., and Hemley, R.J. (2005) Sound velocities of hot dense iron: Birch's Law revisited. Science, 308, 1892–1894.

Litasov, K.D., and Shatskiy, A.F. (2016) Composition of the Earth's core: A review. Russian Geology and Geophysics, 57, 22–46.

Mermin, N.D. (1965) Thermal Properties of the Inhomogeneous Electron Gas. Physical Review, 137, A1441–A1443.

Mori, Y., Ozawa, H., Hirose, K., Sinmyo, R., Tateno, S., Morard, G., and Ohishi, Y. (2017) Melting experiments on Fe–Fe3S system to 254 GPa. Earth and Planetary Science Letters, 464, 135–141.

Murnaghan, F.D. (1944) The Compressibility of Media under Extreme Pressures. Proceedings of the National Academy of Sciences of the United States of America, 30, 244–247.

Nosé, S. (1984) A molecular dynamics method for simulations in the canonical ensemble. Molecular Physics, 52, 255–268.

Perdew, J.P., Burke, K., and Ernzerhof, M. (1996) Generalized Gradient Approximation Made Simple. Physical Review Letters, 77, 3865–3868.

Poirier, J.P. (1994) Light elements in the Earth's outer core: A critical review. Physics of the Earth and Planetary Interiors, 85, 319–337.

Sanloup, C., Guyot, F., Gillet, P., and Fei, Y. (2002) Physical properties of liquid Fe alloys at high pressure and their bearings on the nature of metallic planetary cores. Journal of Geophysical Research: Solid Earth, 107, ECV 4-1-ECV 4-9.

Seagle, C.T., Campbell, A.J., Heinz, D.L., Shen, G., and Prakapenka, V.B. (2006) Thermal equation of State of Fe3S and implications for sulfur in Earth's core. Journal of Geophysical Research: Solid Earth, 111, 1–7.

Stixrude, L., Wasserman, E., and Cohen, R.E. (1997) Composition and temperature of Earth's inner core. Journal of Geophysical Research: Solid Earth, 102, 24729–24739.

Umemoto, K., and Hirose, K. (2015) Liquid iron-hydrogen alloys at outer core conditions by first-principles calculations. Geophysical Research Letters, 42, 7513–7520.

Umemoto, K., and Hirose, K. (2020) Chemical compositions of the outer core examined by first principles calculations. Earth and Planetary Science Letters, 531, 116009.

355 Umemoto, K., Hirose, K., Imada, S., Nakajima, Y., Komabayashi, T., Tsutsui, S., and Baron,
356 A.Q.R. (2014) Liquid iron-sulfur alloys at outer core conditions by first-principles
357 calculations. Geophysical Research Letters, 41, 6712–6717.
358 Vočadlo, L., Alfè, D., Gillan, M.J., and Price, G.D. (2003) The properties of iron under core
359 conditions from first principles calculations. Physics of the Earth and Planetary Interiors,
360 140, 101–125.
361 Wagle, F., and Steinle-Neumann, G. (2019) Liquid Iron Equation of State to the Terapascal
362 Regime From Ab Initio Simulations. Journal of Geophysical Research: Solid Earth, 124,
363 3350–3364.
364 Wasserman, E., Stixrude, L., and Cohen, R.E. (1996) Thermal properties of iron at high
365 pressures and temperatures. Physical Review B, 53, 8296–8309.
366 Zhang, Y., Sekine, T., He, H., Yu, Y., Liu, F., and Zhang, M. (2016) Experimental
367 constraints on light elements in the Earth's outer core. Scientific Reports, 6, 22473.
368
369

370 # Figure captions

371 **Figure 1** The density of liquid Fe at 6000 K is compared with reported data. (a) is
372 experimental solid hcp Fe (Dewaele et al. 2006). (b) is first-principles calculation at 6000 K
373 (Umemoto et al. 2014). (d) is experimental liquid Fe at 6000 K derived from parameterized
374 EOS (Anderson and Ahrens 1994). The filled blue square is density at 6000 K, 260 GPa by
375 shock-wave experiment (Brown and McQueen 1986).

376 **Figure 2** Isothermal density as a function of pressure for liquid Fe–S alloys. PREM is
377 included for comparison (Dziewonski and Anderson 1981). The cubic, circle, and up-/down-
378 triangle symbols are FP-MD $P–T–V$ data. The red, green, blue, and magenta solid lines are
379 the data from Murnaghan (M) EOS.

380 **Figure 3** Isothermal sound velocity profiles of liquid Fe–S alloys. PREM is included for
381 comparison (Dziewonski and Anderson 1981).

382 **Figure 4 A**diabatic temperatures profiles in the outer core with four different anchoring
383 temperatures (Boehler 1993; Stixrude et al. 1997; Belonoshko et al. 2000; Laio et al. 2000;
384 Alfè 2009; Anzellini et al. 2013).

385 **Figure 5** Density and sound velocity as a function of pressure along the geotherm. Open
386 squares are shock-wave experimental data by Huang (Huang et al. 2018). Open triangles
387 represent data from first-principles calculation by Umemoto (Umemoto et al. 2014).

388

389 Table 1 Murnaghan-MGD EOS parameters for liquid Fe–S alloys

parameters	V_0 (Å^3/atom)	K_{T0} (GPa)	K_{T0}'	γ_0	e_0 (K^{-1})	g
Fe	13.55	137.96	3.42	1.50	1.16491083e–04	1.12396676e+00
Fe–5.5wt.%S ($Fe_{98}S_{10}$)	13.99	117.79	3.46	1.50	–4.00572800e–05	1.19346252e+00
Fe–11.5wt.%S ($Fe_{88}S_{20}$)	14.37	107.38	3.40	1.50	–2.88105736e–05	5.06933449e–01
Fe–18.1wt.%S ($Fe_{78}S_{30}$)	15.68	75.15	3.46	1.50	–5.10315845e–05	1.61538473e+00

390 Note: the parameters are fitted based on the reference temperature 6000 K.
391
392

393

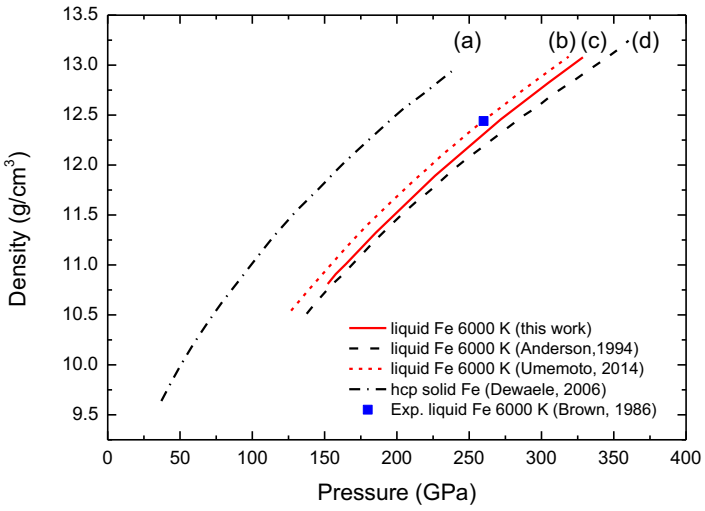

394

395 **Figure 1**

396

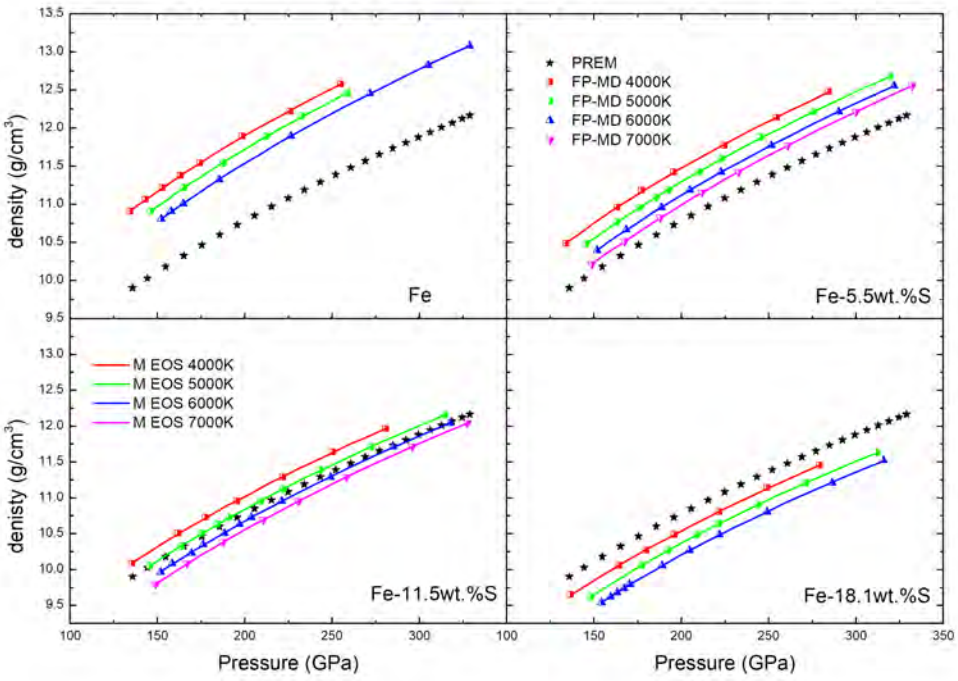
density (g/cm^3)
Pressure (GPa)
Fe
Fe-5.5wt.%S
Fe-11.5wt.%S
Fe-18.1wt.%S
PREM
FP-MD 4000K
FP-MD 5000K
FP-MD 6000K
FP-MD 7000K
M EOS 4000K
M EOS 5000K
M EOS 6000K
M EOS 7000K

Figure 2

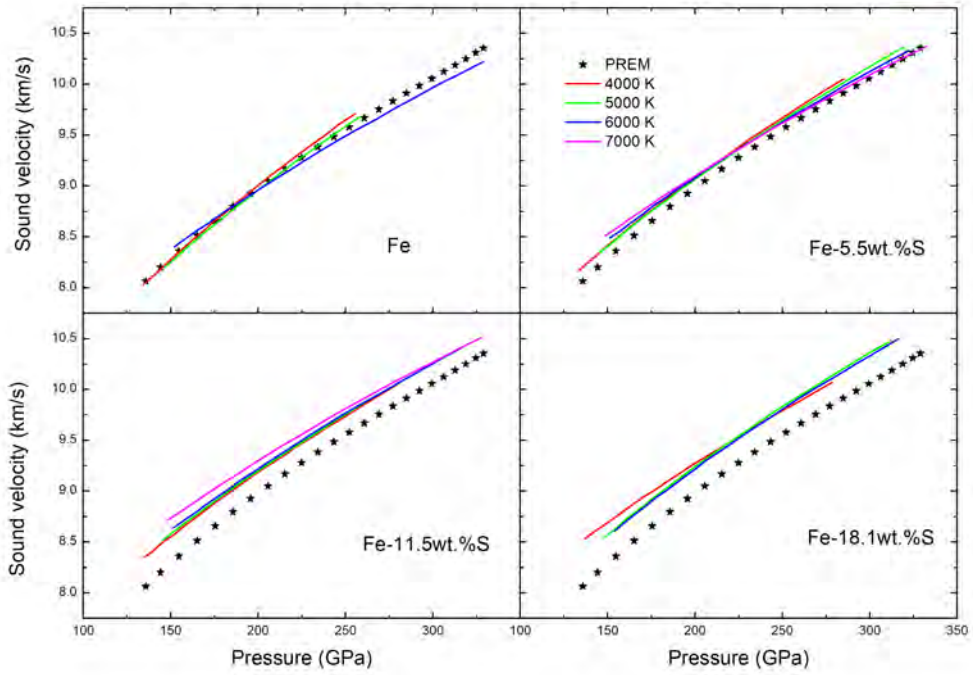
Sound velocity (km/s)
Pressure (GPa)
PREM
4000 K
5000 K
6000 K
7000 K
Fe
Fe-5.5wt.%S
Fe-11.5wt.%S
Fe-18.1wt.%S

Figure 3

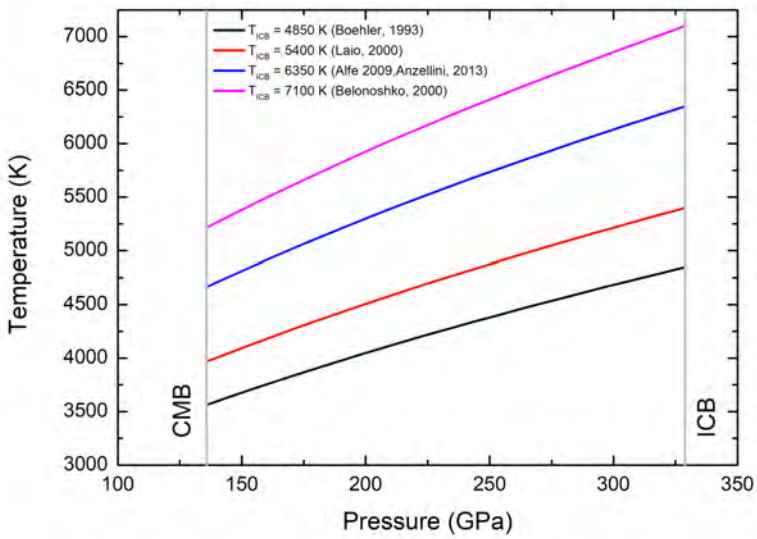
T_{ICB} = 4850 K (Boehler, 1993)
T_{ICB} = 5400 K (Laio, 2000)
T_{ICB} = 6350 K (Alfe 2009,Anzellini, 2013)
T_{ICB} = 7100 K (Belonoshko, 2000)
Temperature (K)
Pressure (GPa)
CMB
ICB
7000
6500
6000
5500
5000
4500
4000
3500
3000
100
150
200
250
300
350

Figure 4.

.

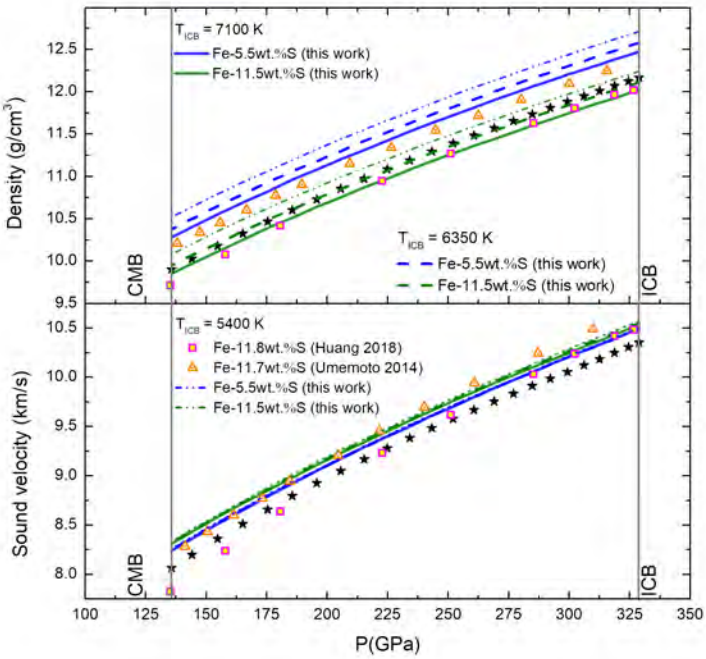
T_ICB = 7100 K
Fe-5.5wt.%S (this work)
Fe-11.5wt.%S (this work)
T_ICB = 6350 K
Fe-5.5wt.%S (this work)
Fe-11.5wt.%S (this work)
Density (g/cm³)
CMB
ICB
T_ICB = 5400 K
Fe-11.8wt.%S (Huang 2018)
Fe-11.7wt.%S (Umemoto 2014)
Fe-5.5wt.%S (this work)
Fe-11.5wt.%S (this work)
Sound velocity (km/s)
CMB
ICB
P(GPa)

Figure 5